



Cite this: DOI: 10.1039/c7dt02144e

Triaminoborane-bridged diphosphine complexes with Ni and Pd: coordination chemistry, structures, and ligand-centered reactivity†

Kyoungsoon Lee, Courtney M. Donahue and Scott R. Daly *

The synthesis, coordination chemistry, and reactivity of two diphosphines containing the cyclic triaminoborane 1,8,10,9-triazaboradecalin (TBD) are described. To evaluate the ligand-centered reactivity of ${}^{\text{P}^{\text{h}}}\text{TBDPhos}$ and ${}^{\text{iPr}}\text{TBDPhos}$, the complexes $({}^{\text{P}^{\text{h}}}\text{TBDPhos})\text{MCl}_2$ and $({}^{\text{iPr}}\text{TBDPhos})\text{MCl}_2$, where $\text{M} = \text{Ni}$ and Pd , were prepared and characterized by elemental analysis, multinuclear NMR spectroscopy (${}^1\text{H}$, ${}^{13}\text{C}$, ${}^{31}\text{P}$, and ${}^{11}\text{B}$), and single-crystal X-ray diffraction (XRD). Despite very low boron Lewis acidity in the TBD backbone, $({}^{\text{P}^{\text{h}}}\text{TBDPhos})\text{NiCl}_2$ (**1**) and $({}^{\text{P}^{\text{h}}}\text{TBDPhos})\text{PdCl}_2$ (**3**) react with H_2O , alcohols, and hydrated fluoride reagents in the presence of NEt_3 to yield *trans* H–O or H–F addition across the bridgehead N–B bond. In contrast, ${}^{\text{iPr}}\text{TBDPhos}$ shows no appreciable reactivity when bound to NiCl_2 (**2**) and PdCl_2 (**4**), which is attributed to the sterically-bulky isopropyl substituents blocking substrate access to boron in the TBD backbone. The new complexes $\{[({}^{\text{P}^{\text{h}}}\text{TBDPhos-H}_2\text{O})\text{Ni}]_2(\mu\text{-OH})_2\}\text{Cl}_2$ (**5**), $\{[({}^{\text{P}^{\text{h}}}\text{TBDPhos-H}_2\text{O})\text{Pd}]_2(\mu\text{-OH})_2\}\text{Cl}_2$ (**6**), $({}^{\text{P}^{\text{h}}}\text{TBDPhos-MeOH})\text{NiCl}_2$ (**7**), $({}^{\text{P}^{\text{h}}}\text{TBDPhos-MeOH})\text{PdCl}_2$ (**8**), $({}^{\text{P}^{\text{h}}}\text{TBDPhos-C}_3\text{H}_5\text{OH})\text{PdCl}_2$ (**9**), and $\{[({}^{\text{P}^{\text{h}}}\text{TBDPhos-HF})\text{Ni}]_2(\mu\text{-OH})_2\}\text{Cl}_2$ (**10**) were isolated, and all but **6** were structurally characterized by single-crystal XRD. Multinuclear NMR studies revealed that isolated, crystallographically-authenticated samples of **5–9** lose ligand-bound water or alcohol with reappearance of starting materials **1** and **3** when dissolved in NMR solvents. Addition of NEt_3 attenuated the water and alcohol loss from **5–9** to allow ${}^1\text{H}$, ${}^{13}\text{C}$, ${}^{31}\text{P}$, and ${}^{11}\text{B}$ NMR data to be collected for all the compounds, confirming the determined structures. Additional reactivity experiments with NaOMe and fluoride reagents suggested that participation of the bridgehead nitrogen in the TBD backbone is important for promoting reactivity at boron when ${}^{\text{P}^{\text{h}}}\text{TBDPhos}$ is bound to Ni and Pd. The term “cooperative ligand-centered reactivity” (CLR) is proposed to define chemical reactions that appear to require participation of more than one atom on the ligand, such as those reported here.

Received 12th June 2017,
Accepted 30th June 2017

DOI: 10.1039/c7dt02144e

rsc.li/dalton

Introduction

The incorporation of trisubstituted boranes in multidentate ligand platforms has allowed new types of cooperative metal–ligand transformations, as well as other forms of ligand-centered reactivity to be realized.^{1–5} These reactions often exploit the vacant p-orbital on boron, which can accept electron density from Lewis bases, nucleophiles, and electron-rich metals. Borane ligand function and reactivity are typically governed by Lewis acidity and position of boron in the ligand scaffold. Boratranes and related ambiphilic ligands,^{6,7} for

example, are configured so that the boron can form Z-type interactions with metals, thereby providing access to small molecule transformations *via* cooperative metal–ligand reactions (Chart 1). Other ligand designs rely on locating the borane in the second coordination sphere to serve as a remote Lewis acid binding site. This latter approach has been used in diverse applications, including catalysis and optical sensing of fluoride and cyanide.^{8–12}

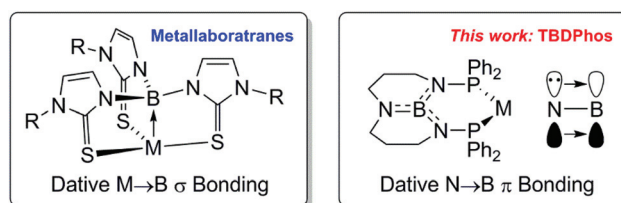


Chart 1 Structural comparison of triaminoboranes in $[\kappa^4\text{-B(mim)}_3]\text{M}$ and TBDPhos complexes reported here.

The University of Iowa, Department of Chemistry, E331 Chemistry Building, Iowa City, IA 52242-1294, USA. E-mail: scott-daly@uiowa.edu

† Electronic supplementary information (ESI) available: Molecular structure of **3** and NMR spectra. Tabulated crystallographic details and data in CIF format. CCDC 1511356–1511359 and 1550914–1550920. For ESI and crystallographic data in CIF or other electronic format see DOI: 10.1039/c7dt02144e

We recently began investigating triaminoborane ligands with the goals of accessing new forms of ligand-centered reactivity and overcoming challenges associated with the high oxophilicity of more Lewis-acidic organoboranes in cooperative metal–ligand reactions.^{13,14} Triaminoboranes are poor Lewis acids: they have dramatically lower Lewis acidity than trialkyl- and triarylboranes,^{15,16} especially those commonly encountered in frustrated Lewis pair chemistry (*e.g.*, $B(C_6F_5)_3$).^{17–22} The decreased Lewis acidity stems from donation of the nitrogen lone pairs into the vacant p-orbital on boron, which imparts significant N–B double-bond character.²³ The low Lewis acidity of triaminoboranes, however, does not necessarily imply a lack of reactivity when used in ligands: $[\kappa^4-B(mim^R)_3]M$ and related complexes have been shown to form dative $M \rightarrow B$ σ bonds (*i.e.*, Z-type bonds) that, in some instances, facilitate reactivity across the metal and boron (Chart 1).^{24–37} We postulated that similar cooperative reactivity could be achieved across dative $N \rightarrow B$ π bonds on the ligand if the triaminoborane was reconfigured to prevent interactions with the metal.³⁸

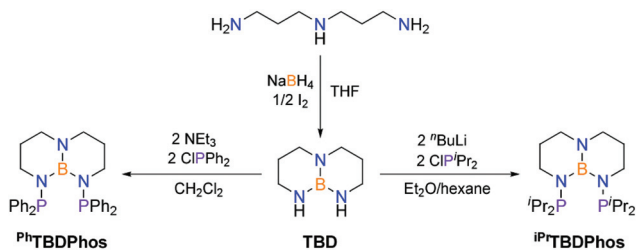
To test our hypothesis, we prepared two diphosphines derived from a cyclic triaminoborane called 1,8,10,9-triazaboradecalin (TBD; Scheme 1).^{39,40} The flexible, chelating triamino framework in TBD was selected to (1) prevent ligand decomposition and boron loss *via* dissociative B–N bond cleavage, and (2) accommodate the anticipated trigonal planar-to-tetrahedral distortions at boron during reactions (*i.e.*, $sp^2 \rightarrow sp^3$). The diphosphine scaffold was selected because (1) it prevents TBD

from interacting with the metal, and (2) diphosphines provide access to coordination chemistry with a wide range of transition metals. As we will show, despite the remote location and low Lewis acidity, the bridgehead nitrogen in the TBD backbone helps facilitate new ligand-centered reactions at boron when coordinated to Ni and Pd.

Results and discussion

TBD was prepared by refluxing 3,3'-diaminodipropylamine with $NaBH_4$ and I_2 in THF for several days, as described previously (Scheme 1).⁴¹ It was then treated with $ClPR_2$ ($R = Ph$ or iPr) in the presence of base to yield the new diphosphines $^{Ph}TBDPhos$ and $^{iPr}TBDPhos$, as confirmed by multinuclear NMR spectroscopy and single-crystal X-ray diffraction (Fig. 1). The ^{11}B NMR resonance of TBD at δ 22.4 in $CDCl_3$ shifts downfield slightly to δ 26.2 and 25.8 in $^{Ph}TBDPhos$ and $^{iPr}TBDPhos$, respectively, and new ^{31}P NMR resonances were observed at δ 47.7 and 61.3 (Table 1). XRD data confirmed sp^2 hybridization at boron in both diphosphines, as indicated by the 360.0° sum of the three N–B–N angles (Table 2). The bridgehead N–B bond distances of 1.415(3) and 1.414(3) Å, respectively, are 0.03–0.04 Å shorter than the N–B distances for N atoms bound to P. For comparison, the N–B bond distances in $B(NMe_2)_3$ range from 1.43–1.44 Å.⁴²

We next established the coordination chemistry of TBD-bridged diphosphines with $NiCl_2$ and $PdCl_2$. Treatment of $(DME)NiCl_2$ ($DME = 1,2$ -dimethoxyethane) with $^{Ph}TBDPhos$ or $^{iPr}TBDPhos$ in CH_2Cl_2 yielded $(^{Ph}TBDPhos)NiCl_2$ (1) or $(^{iPr}TBDPhos)NiCl_2$ (2), respectively. A similar reaction, starting from $(PhCN)_2PdCl_2$, was used to prepare $(^R TBDPhos)PdCl_2$, where $R = Ph$ (3) or iPr (4). All four compounds were crystallized in good yield from Et_2O/CH_2Cl_2 (70–79%). The ^{11}B NMR resonances are similar to those observed for the free ligands and range from δ 23.9–24.5, whereas the ^{31}P NMR resonances shift downfield from δ 47.7 ($^{Ph}TBDPhos$) and 61.3 ($^{iPr}TBDPhos$) upon metalation to 70.1 (1), 147.0 (2), 68.7 (3), and 97.4 (4). The ^{31}P NMR resonance for $(^{iPr}TBDPhos)NiCl_2$ is very broad compared to $(^{Ph}TBDPhos)NiCl_2$ (FWHM = 1200 Hz



Scheme 1 Synthesis of TBD, $^{Ph}TBDPhos$, and $^{iPr}TBDPhos$.

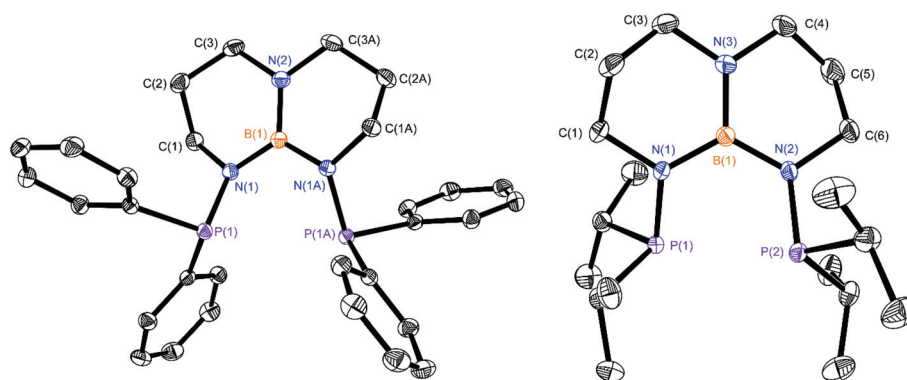


Fig. 1 Molecular structures of $^{Ph}TBDPhos$ (left) and $^{iPr}TBDPhos$ (right) with thermal ellipsoids drawn at the 35% probability level. Hydrogen atoms were omitted from the figure.

Table 1 ^{11}B and ^{31}P NMR resonances for compounds reported herein. Chemical shifts are reported in δ units relative to $\text{BF}_3 \cdot \text{Et}_2\text{O}$ (^{11}B) and $85\% \text{H}_3\text{PO}_4$ (^{31}P)

Compound	^{11}B	$^{31}\text{P}\{\text{H}\}$	Solvent
TBD	22.4	—	CDCl_3
$^{\text{Ph}}\text{TBDPhos}$	26.2	47.7	CDCl_3
$^{\text{iPr}}\text{TBDPhos}$	25.8	61.3	CDCl_3
1	23.9	70.1	CDCl_3
2	24.5	147.0	CDCl_3
3	24.2	68.7	CDCl_3
4	24.5	97.4	CDCl_3
5	1.0	70.8	CDCl_3
6	1.8	65.3	CD_2Cl_2
7	1.9	69.8	CDCl_3
8	3.2	64.5	$\text{DMSO-}d_6$
9	2.9	66.1	CD_2Cl_2
10	1.6	72.0	CDCl_3

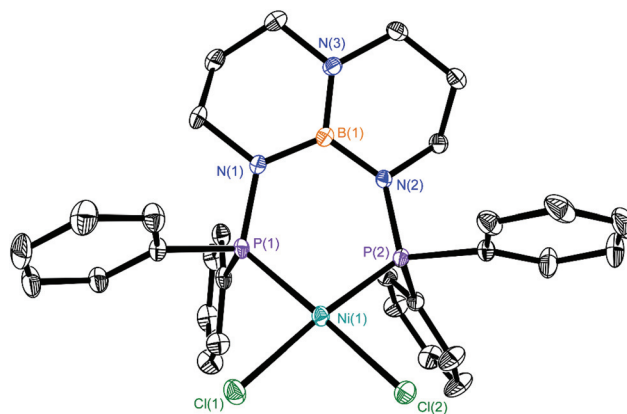


Fig. 2 Molecular structure of $(^{\text{Ph}}\text{TBDPhos})\text{NiCl}_2$ (**1**) with thermal ellipsoids drawn at the 35% probability level. Hydrogen atoms were omitted from the figure. The molecular structure of the isomorphous Pd congener **3** is provided in the ESI (Fig. S1†).

vs. 130 Hz), suggesting that the Ni adopts a paramagnetic, high-spin d^8 electron configuration in contrast to the low spin d^8 configuration in **1**, **3**, and **4**. The change in electron configuration and corresponding structural distortion from square planar (low spin) to tetrahedral (high spin) is common for $\text{Ni}(\text{II})$ phosphine complexes, especially those with bulky substituents.⁴³

Single-crystal XRD studies confirmed the identities of **1–4** (Fig. 2 and 3). As the NMR data suggested, **1**, **3**, and **4** adopt low spin, square planar coordination geometries whereas $(^{\text{iPr}}\text{TBDPhos})\text{NiCl}_2$ (**2**) is distorted tetrahedral. The chloride ligands in **2** are rotated 50° out of the plane defined by the Ni and P atoms. As reported for other $\text{Ni}(\text{II})$ phosphine complexes, we suspected that the tetrahedral distortion was attributed to the greater steric demands of isopropyl substituents in **2** coupled with the energetically accessible high spin configuration of $\text{Ni}(\text{II})$.^{43–45} Evidence of the increased steric profile of $^{\text{iPr}}\text{TBDPhos}$ compared to $^{\text{Ph}}\text{TBDPhos}$ is provided by comparison of the Pd bond angles in **3** and **4**: the P–Pd–P angle

increased from $88.47(2)^\circ$ in $(^{\text{Ph}}\text{TBDPhos})\text{PdCl}_2$ to $95.32(2)^\circ$ in $(^{\text{iPr}}\text{TBDPhos})\text{PdCl}_2$, and the Cl–Pd–Cl angle decreased from $89.47(2)^\circ$ to $85.80(2)^\circ$. Despite the angular variations, no significant differences were observed in the Pd–P and Pd–Cl bond distances. Collectively, the metal–ligand bond distances in **1–4** are comparable to other NiCl_2 and PdCl_2 complexes with phenyl- and isopropyl-substituted diphosphines.⁴⁶ As shown in Table 2, only subtle differences were observed in the ligand bond distances and angles upon metallation.

Once we established the syntheses of **1–4**, we began investigating their reactivity. We first tested the Lewis acidity of TBD and $^{\text{Ph}}\text{TBDPhos}$ in C_6D_6 , and **1** in CD_2Cl_2 using the Gutmann–Beckett method.^{15,16} No change was observed in the ^{31}P NMR shift of OPEt_3 due to $\text{B} \leftarrow \text{OPEt}_3$ interactions, thus confirming their very low Lewis acidity.⁴⁷ We next investigated the hydrolysis susceptibility of free and bound $^{\text{Ph}}\text{TBDPhos}$ (Scheme 2). A solution of **1** in CDCl_3 was layered with excess water in air and

Table 2 Selected bond distances and angles for $^{\text{Ph}}\text{TBDPhos}$, $^{\text{iPr}}\text{TBDPhos}$, **1–5**, and **7–10** from single-crystal XRD data (X = Cl or O and Y = O or F)

	$^{\text{Ph}}\text{TBDPhos}$	$^{\text{iPr}}\text{TBDPhos}$	1	2	3	4	5	7	8	9	10 ^a
M–P	—	—	2.1463(6)	2.1349(5)	2.2311(5)	2.2421(7)	2.1131(9)	2.1538(8)	2.2227(9)	2.2286(5)	2.1309(6)
	—	—	2.1556(6)	—	2.2334(6)	2.2430(6)	2.110(1)	2.146(1)	2.2331(6)	2.2368(4)	2.1357(8)
M–X	—	—	2.2070(7)	2.2149(5)	2.3550(5)	2.3666(6)	1.882(2)	2.2000(8)	2.367(1)	2.3599(5)	1.892(2)
	—	—	2.2087(6)	—	2.3604(6)	2.3667(7)	1.899(3)	2.207(1)	2.3566(8)	2.3710(6)	1.900(2)
P–N	1.707(1)	1.715(1)	1.678(2)	1.687(1)	1.671(1)	1.679(2)	1.638(3)	1.660(3)	1.649(2)	1.654(1)	1.649(2)
	—	1.718(1)	1.672(2)	—	1.679(1)	1.681(2)	1.645(3)	1.655(3)	1.654(2)	1.656(1)	1.650(2)
B–N	1.418(3)	1.422(2)	1.408(3)	1.413(3)	1.415(2)	1.418(3)	1.645(4)	1.650(4)	1.661(4)	1.658(2)	1.613(3)
B–N(P)	1.448(2)	1.447(2)	1.454(3)	1.459(2)	1.460(2)	1.453(3)	1.525(5)	1.514(3)	1.523(3)	1.520(2)	1.510(3)
	—	1.451(2)	1.454(3)	—	1.460(2)	1.458(3)	1.542(4)	1.516(4)	1.526(4)	1.525(2)	1.513(3)
B–Y	—	—	—	—	—	—	1.427(4)	1.450(4)	1.442(3)	1.452(2)	1.424(3)
P–M–P	—	—	92.91(2)	95.94(3)	88.47(2)	95.32(2)	92.77(3)	96.39(3)	95.35(3)	95.44(2)	89.66(3)
X–M–X	—	—	90.45(2)	96.69(3)	89.47(2)	85.80(2)	78.2(1)	89.85(4)	88.53(3)	88.67(2)	77.06(7)
P–M–X	—	—	87.54(2)	95.02(2)	90.45(2)	89.49(2)	94.17(8)	85.88(4)	86.63(3)	86.89(2)	96.43(5)
	—	—	92.91(2)	143.36(2)	91.07(2)	89.44(2)	94.86(8)	88.02(3)	89.71(3)	89.05(2)	96.77(5)
	—	—	170.78(2)	—	172.94(2)	174.92(2)	170.85(8)	175.18(4)	174.47(3)	175.29(2)	173.47(6)
	—	—	177.85(2)	—	175.50(2)	175.00(2)	172.37(8)	175.46(4)	174.50(3)	176.79(2)	173.19(5)
$\sum\text{NBN}$	360.0(1)	360.1(1)	359.9(2)	360.0(2)	360.0(1)	360.0(1)	322.2(3)	327.5(2)	327.0(2)	328.4(1)	331.5(2)

^a Values from one half of the asymmetric dimer. Values for the other half of the dimer are similar.

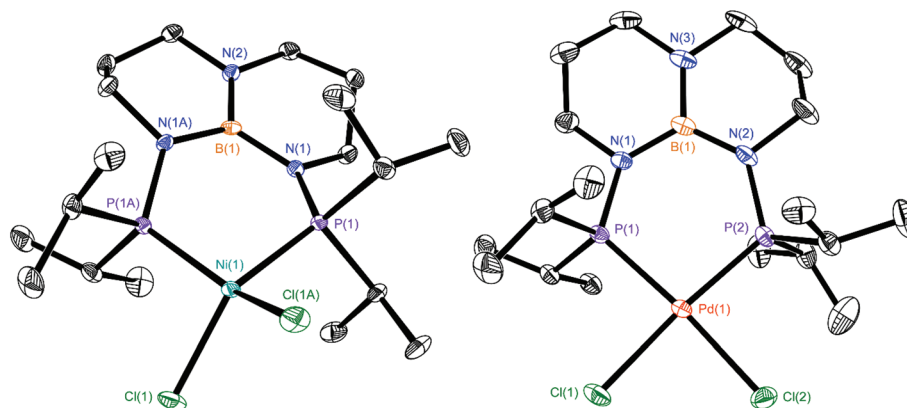
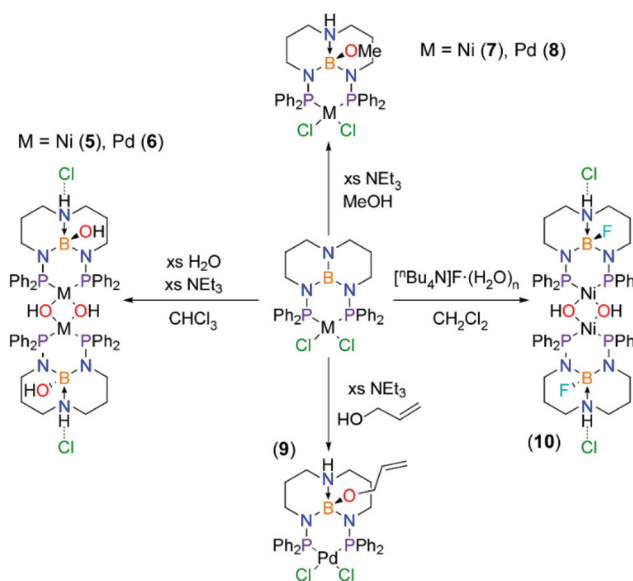


Fig. 3 Molecular structures of (iPrTBDPhos)NiCl₂ (2; left) and (iPrTBDPhos)PdCl₂ (4; right) with thermal ellipsoids drawn at the 35% probability level. Hydrogen atoms were omitted from the figure.



Scheme 2 Reactivity studies of (Ph^hTBDPhos)MCl₂ (M = Ni or Pd).

monitored by ³¹P and ¹¹B NMR spectroscopy. Approximately half of the Ph^hTBDPhos in **1** reacted with H₂O over the course of two days, as indicated by new resonances in the ¹¹B and ³¹P NMR spectra at δ 1.0 and 70.8, respectively. The relatively large upfield shift in the ¹¹B NMR spectrum (22.9 ppm) is known to be diagnostic for a change from three-coordinate to four-coordinate boron.⁴⁸ These results are notable when compared to reaction of H₂O with free Ph^hTBDPhos under identical conditions: the ligand decomposes, as is indicated by the disappearance of Ph^hTBDPhos NMR resonances and appearance of B(OH)₃ in the water layer.

We discovered that the reaction of **1** with water could be expedited by adding excess NEt₃, which resulted in immediate and quantitative conversion to the new species observed previously in the ¹¹B NMR spectrum at δ 1.0. Single-crystal XRD studies on crystals grown by vapor diffusion of pentane into CHCl₃ or CDCl₃ revealed the complex to be {[(Ph^hTBDPhos-H₂O)

Ni]₂(μ-OH)₂Cl₂ (**5**; Fig. 4). The dimeric structure of **5** contains two Ni ions bridged by hydroxide ligands, but the most notable change was observed at the TBD backbone: a water molecule was added across the bridgehead N-B bond to give *trans* B-OH and N-H. In response, the bridgehead N-B bond elongated from 1.415(3) Å in **1** to 1.645(4) Å in **5**, consistent with transformation of the covalent N-B bond to a dative N→B bond. For comparison, N→B bond lengths for the archetypal dative complex Me₂NH·BH₃ and the more closely related Me₂NH·B(methimazolyl)₃ are 1.5965(13) and 1.605(3) Å, respectively.^{49,50} The remaining N-B distances in **5** increased by *ca.* 0.1 Å, corresponding to the loss of partial N-B double-bond character and a geometric change from trigonal planar to tetrahedral boron (*i.e.*, sp² to sp³). Half the chlorides originating from **1** remained in the outer coordination sphere of **5**, balancing the unquenched charge on each Ni(II).

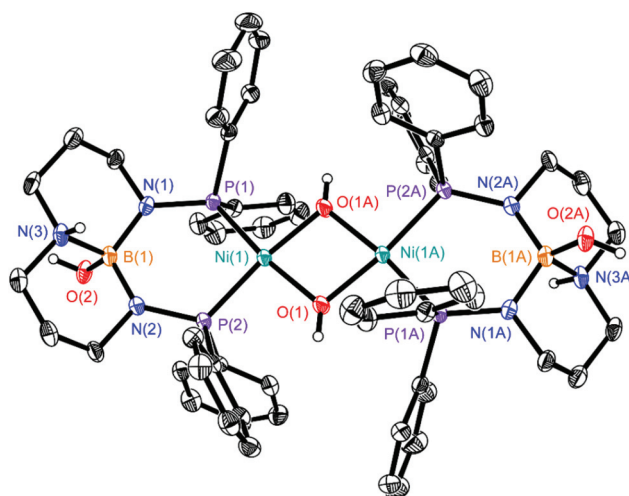
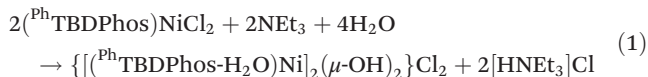


Fig. 4 Molecular structure of {[(Ph^hTBDPhos-H₂O)Ni]₂(μ-OH)₂Cl₂ (**5**) with thermal ellipsoids drawn at the 35% probability level. The outer-sphere chloride and hydrogen atoms attached to carbon were omitted from the figure.

The exact role of the NEt_3 in the accelerated production of **5** is under investigation, but it is evident that formation of OH^- with elimination of $[\text{HNEt}_3]\text{Cl}$ is important to the overall reaction. A proposed balanced reaction for the synthesis of **5** is provided in eqn (1).



$[\text{HNEt}_3]\text{Cl}$ was isolated from the reaction mixtures, confirming its proposed formation. The arrangement of N–H and B–OH on opposite faces of the TBD backbone suggests that NEt_3 may play a role in shuttling the bridgehead N–H proton *trans* to the B–OH in a stepwise process. Also relevant, the bridgehead nitrogen in **5** remains protonated despite the use of excess NEt_3 , suggesting that the bridgehead nitrogen in $\text{Ph}^{\text{TBDPhos}}$ is more basic.

^1H NMR data collected on crystalline samples of **5** in CDCl_3 revealed three new peaks assigned to N–H, B–OH, and Ni–OH at δ 8.44, 0.25, and -4.48 , respectively. The upfield Ni–OH assignment is similar to the upfield shift reported for $[(\text{dippe})\text{Ni}(\mu\text{-OH})_2](\text{PF}_6)_2$ at $\delta -1.59$.⁵¹ The three propylene ^1H resonances that form the TBD backbone in **1** at 1.37, 2.80, and 3.05 split into six diastereotopic resonances in **5**, as expected due to the loss of the BN_3 mirror plane. In addition to resonances assigned to **5**, the ^1H NMR data revealed smaller resonances in the baseline that increased in intensity over time. We discovered that addition of NEt_3 to NMR samples of **5** in CDCl_3 attenuated the in-growth of these smaller resonances and increased the solubility of **5** so that ^{13}C NMR data could be collected overnight. The ^{13}C NMR spectrum revealed resonances consistent with **5**, but also captured the slow in-growth of resonances matching those previously observed for **1** (Fig. 5). The ^{11}B NMR spectrum collected after the overnight ^{13}C NMR data acquisition showed a broad feature at δ 23.9 that corroborated the reappearance of **1** (Fig. 5; right inset). The resonance at δ 23.9 was not observed in the ^{11}B NMR spectrum collected immediately before the ^{13}C NMR data collection. These results suggested that **5** was losing H_2O from the TBD backbone when removed from wet solvent, and is notable given that irrevers-

ible B–O bond formation is known to limit the utility of some trisubstituted borane ligands in catalytic reactions.¹⁴

As shown in eqn (1), half of the chloride ligands from **1** were removed *via* production of $[\text{HNEt}_3]\text{Cl}$ in the synthesis of **5**. Hence, we postulated that addition of excess $[\text{HNEt}_3]\text{Cl}$ to solutions of **5** could be used to quantitatively form **1**. Indeed, ^{31}P and ^{11}B resonances assigned to **5** disappeared after addition of excess $[\text{HNEt}_3]\text{Cl}$ and resonances assigned to **1** reappeared (Fig. 6). The reaction, however, is not quantitative, as indicated by a small unidentified peak in the ^{31}P NMR spectrum at δ 27.5 attributed to $\text{Ph}^{\text{TBDPhos}}$ decomposition (*vide infra*). The new ^{11}B and ^{31}P NMR resonances of δ 23.7 and 68.4, respectively, are slightly different than those observed for **1** in CDCl_3 , but are identical to those obtained when excess $[\text{HNEt}_3]\text{Cl}$ was added to CDCl_3 solutions of **1**. The small differences in the NMR spectra of **1** in the presence and absence of $[\text{HNEt}_3]\text{Cl}$ may be attributed to changes in TBD protonation in $(\text{Ph}^{\text{TBDPhos}})\text{NiCl}_2$ in solution. However, despite repeated attempts, no compounds other than **1** and $[\text{HNEt}_3]\text{Cl}$ were isolated from these mixtures.

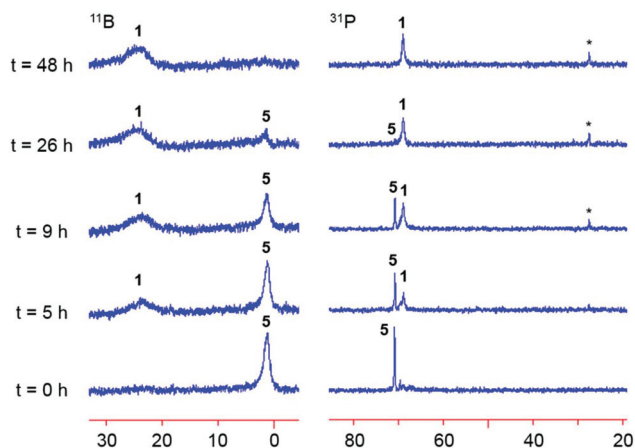


Fig. 6 ^{11}B (left) and ^{31}P (right) NMR spectra collected at specified intervals over 48 h for the reaction of **5** with excess $\text{NEt}_3\text{-HCl}$ in CDCl_3 . The asterisks indicates the ^{31}P NMR resonance assigned to decomposition of $\text{Ph}^{\text{TBDPhos}}$.

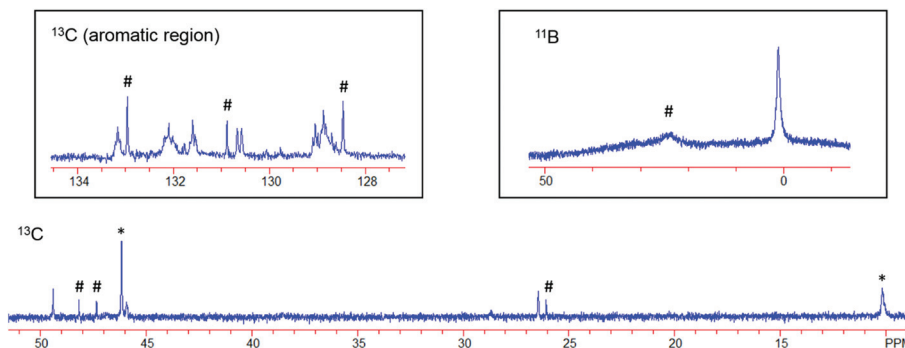


Fig. 5 ^{13}C and ^{11}B NMR spectra of $\{[(\text{Ph}^{\text{TBDPhos}}\text{-H}_2\text{O})\text{Ni}]_2(\mu\text{-OH})_2\}\text{Cl}_2$ (**5**) collected in CDCl_3 . The ^{11}B NMR spectrum was collected at the end of the overnight ^{13}C data collection. The * symbol indicates resonances assigned to added NEt_3 , and the # symbol indicates resonances assigned to **1**.

Next we explored the effect of metal identity on $^{\text{Ph}}\text{TBDPhos}$ reactivity by treating ($^{\text{Ph}}\text{TBDPhos}$)PdCl₂ (**3**) with water in the presence of NEt₃, as described previously for the synthesis of **5**. The reaction yielded mixtures from which the hydroxide-bridged Pd congener $\{[(^{\text{Ph}}\text{TBDPhos-H}_2\text{O})\text{Pd}]_2(\mu\text{-OH})_2\}\text{Cl}_2$ (**6**) could be obtained (Scheme 2). As with the Ni congener **5**, ^{31}P and ^{11}B NMR spectra collected on the reaction mixtures revealed only single resonances assigned to **6** at δ 65.3 and 1.8, respectively. Crystals grown from the reaction mixtures did not yield XRD data suitable for publication, but were sufficient to confirm the dimeric structure and *trans* water addition across the backbone. The composition of **6** was further corroborated by a sharp bridging Pd–OH peak in the IR spectrum at 3607 cm⁻¹ and a broad B–OH feature centered at 3340 cm⁻¹. As observed with **5**, ^1H and ^{13}C NMR data collected on isolated samples of **6** in CD₂Cl₂ with added NEt₃ yielded resonances consistent with **6**, as well as resonances assigned to **3** that grew in over time. Several small unassigned resonances were also observed in the baseline and were most apparent in the ^1H NMR data (Fig. S33; ESI†). We have so far been unable to determine if these are attributed to intermediate species associated with the reverse transformation from **6** to **3** or ligand decomposition. However, their concentrations remained low in all samples analyzed compared to **6** and **3**.

Once the reactivity of **1** and **3** with H₂O was established, we explored how changing phosphorus substituents affected reactivity at the TBD backbone. Unexpectedly, we discovered that switching the phosphorus substituents from phenyl in **1** and **3** to isopropyl in **2** and **4** effectively shut down TBD reactivity with H₂O, as well as MeOH and fluoride substrates (*vide infra*). We suspected that the increased sterics afforded by the bulky isopropyl groups were likely responsible for the attenuated reactivity. Indeed, analysis of space-filling diagrams generated from the XRD data revealed that the isopropyl substituents in **2** and **4** impede substrate access to boron from both sides of the complex. By comparison, the planar phenyl substituents in **1** and **3** can rotate to provide substrate access (Fig. 7).

We next set out to determine if the reactivity of $^{\text{Ph}}\text{TBDPhos}$ in **1** and **3** could be replicated with other substrates. Dissolving **1** and **3** in neat MeOH with excess NEt₃ quantitatively yielded single ^{11}B NMR resonances at δ 1.9 and 3.2, respectively. Single-crystal XRD studies performed on crystals grown *via* vapor diffusion of Et₂O into the reaction mixtures revealed the monomeric complexes ($^{\text{Ph}}\text{TBDPhos-MeOH}$)NiCl₂ (**7**) and ($^{\text{Ph}}\text{TBDPhos-MeOH}$)PdCl₂ (**8**) (Fig. 8). As in **5** and **6**, **7** and **8** reveal *trans* O–H addition of MeOH across the bridgehead N–B bond. The reactivity could be extended to other alcohols; dissolving **3** in allylic alcohol in the presence of base yielded ($^{\text{Ph}}\text{TBDPhos-C}_3\text{H}_5\text{OH}$)PdCl₂ (**9**), which was isolated and structurally characterized (Fig. 9). Unlike the reactions with water, both chloride ligands from starting materials **1** and **3** remain bound to the metals in **7–9**. The new B–OR bond distances in all three structures were similar at 1.450(4), 1.443(3), and 1.453(2) Å, for **7–9**, respectively, despite differences in metal identity and alcohol substrate. Collectively, the B–OR distances in **7–9** are slightly longer than the B–OH distance in

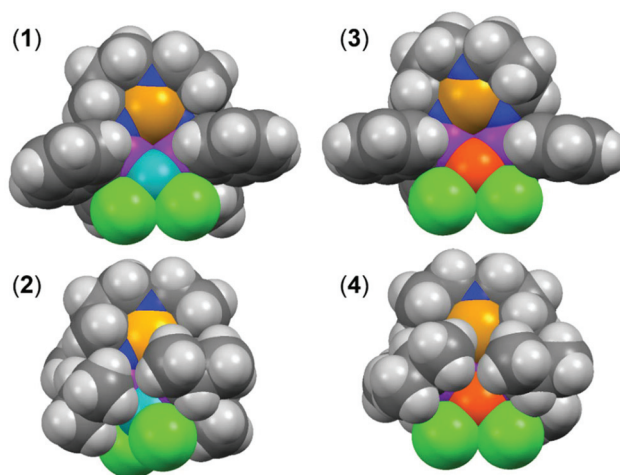


Fig. 7 Space-filling models of ($^{\text{Ph}}\text{TBDPhos}$)NiCl₂ (**1**), ($^{\text{iPr}}\text{TBDPhos}$)NiCl₂ (**2**), ($^{\text{Ph}}\text{TBDPhos}$)PdCl₂ (**3**), and ($^{\text{iPr}}\text{TBDPhos}$)PdCl₂ (**4**) generated using XRD data and the software program Mercury.⁵²

5 at 1.427(4) Å. As observed in the structure of **5**, the bridgehead N–B bond distance elongates to 1.650(4) (**7**), 1.656(3) (**8**), and 1.660(1) Å (**9**), indicative of dative N→B bond formation.

Remarkably, no immediate decomposition of $^{\text{Ph}}\text{TBDPhos}$ was observed despite preparing **7–9** in neat alcohols, but we found that addition of NEt₃ was important for attenuating ligand decomposition over extended reaction times. Stirring **1** in MeOH without NEt₃ for several hours, for example, yielded mixtures that contained **7**, but new resonances were also observed at δ 19.0 and 29.9 in the ^{11}B and ^{31}P NMR spectra, respectively. The ^{11}B resonance at δ 19.0 is consistent with the formation of B(OMe)₃,⁵³ which suggests that the unidentified ^{31}P NMR resonance at δ 29.9 can be assigned to the remaining phosphorus-containing decomposition product. Attempts to isolate the latter product were unsuccessful.

Numerous attempts to collect NMR data on crystallographically-authenticated samples of **7** in anhydrous CDCl₃ yielded, unexpectedly, only ^{31}P and ^{11}B NMR resonances for **1** and the aforementioned ^{31}P NMR peak attributed to $^{\text{Ph}}\text{TBDPhos}$ decomposition (Fig. 10). Similar issues were encountered for **8** and **9**. However, as with our NMR studies of **5** and **6**, we discovered that multinuclear NMR data consistent with the determined structures could be collected in deuterated solvents by adding several equivalents of NEt₃. ^{11}B resonances of **7–9** with cleaved alcohols were shifted downfield several ppm compared to those with water (**5** and **6**), whereas the ^{31}P resonances shifted slightly upfield at δ 69.8 (**7**), 64.5 (**8**), and 66.1 (**9**) (Table 1). The ^1H NMR spectrum of **7** revealed the expected splitting of the $^{\text{Ph}}\text{TBDPhos}$ alkyl and aryl resonances due to the loss of the BN₃ mirror plane. A new sharp singlet associated with B–OMe protons was observed at δ 2.62 and a broad multiplet assigned to the NH proton was located at δ 8.49. Similar diagnostic resonances were assigned in the ^1H NMR spectra of **8** and **9**.

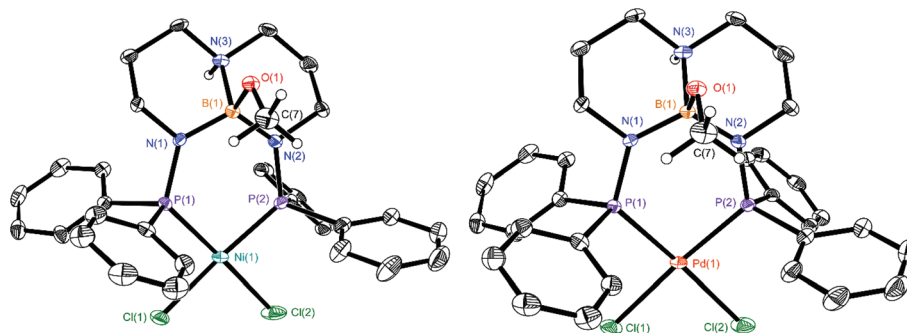


Fig. 8 Molecular structures of (P^hTBDPhos-MeOH)NiCl₂ (7; left) and (P^hTBDPhos-MeOH)PdCl₂ (8; right) with thermal ellipsoids drawn at the 35% probability level. All hydrogen atoms except those attached to nitrogen and the methoxy groups were omitted from the figure.

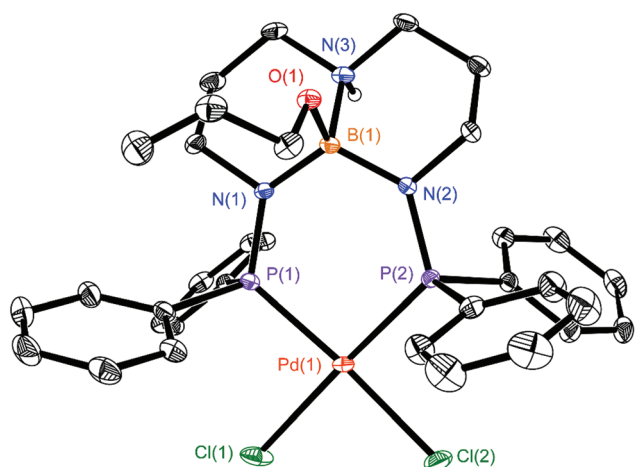


Fig. 9 Molecular structure of (P^hTBDPhos-C₃H₅OH)PdCl₂ (9) with thermal ellipsoids drawn at the 35% probability level. All hydrogen atoms except those attached to nitrogen were omitted from the figure.

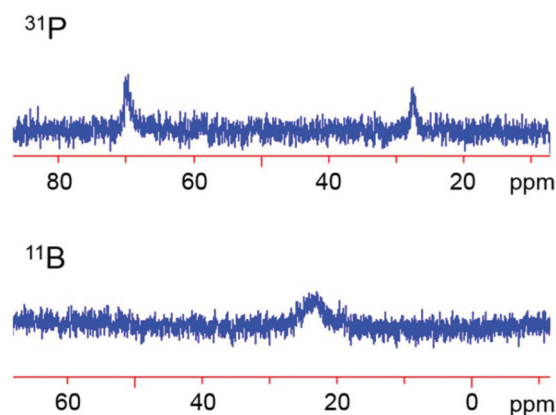


Fig. 10 ³¹P (top) and ¹¹B (bottom) NMR spectra of crystalline (P^hTBDPhos-MeOH)NiCl₂ (7) dissolved in CDCl₃ without NEt₃.

Given that the reactions of **1** and **3** with H₂O and alcohols all resulted in protonation of the bridgehead nitrogen atom in P^hTBDPhos, we postulated that nitrogen participation was important for overcoming the low Lewis acidity of boron in the

TBD backbone. To test our hypothesis, we treated CH₂Cl₂ solutions of **1** with an excess of the anhydrous methoxide salt NaOMe. Despite formation of B-OMe in reactions with MeOH, NaOMe revealed no evidence of methoxide binding to boron after 2 days.

We next tested the reactivity of **1** with fluoride, an anion with a high affinity for Lewis acids. Addition of the anhydrous fluoride source tris(dimethylamino)sulfonium difluorotrimethylsilicate (TASF) to **1** yielded an equilibrium mixture of products containing three- and four-coordinate ¹¹B NMR resonances after 24 hours (Fig. 11). In stark contrast, we found that addition of hydrated fluoride sources such as [nBu₄N]F·(H₂O)_n or addition of TASF in air (*i.e.* in the presence of ambient humidity) yielded rapid formation of {[P^hTBDPhos-HF]Ni}₂(μ-OH)₂Cl₂ (**10**), which was confirmed by multinuclear NMR spectroscopy and single-crystal XRD studies (Fig. 12). As shown in eqn (2), water was cleaved in the reaction to yield the N-H proton on the TBD backbone and the bridging hydroxide ligands.

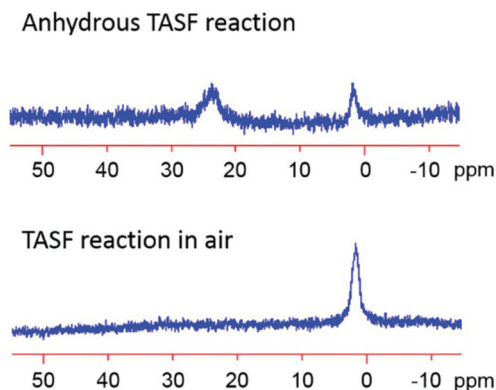
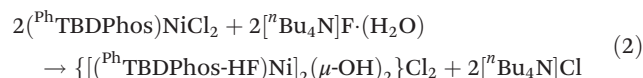


Fig. 11 ¹¹B NMR spectra of reaction mixtures containing **1** and anhydrous TASF (top) and **1** and TASF exposed to ambient humidity in air (bottom). Both spectra were collected in CH₂Cl₂.

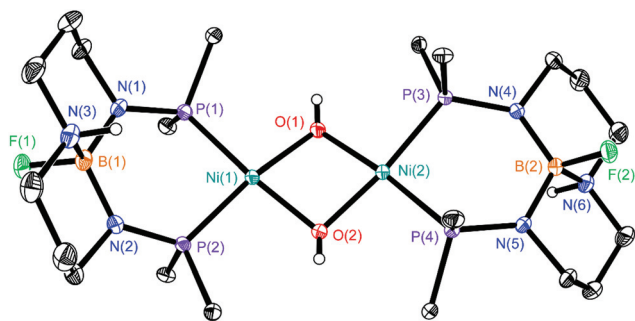


Fig. 12 Molecular structure of $\{[(^{\text{Ph}}\text{TBDPhos-HF})\text{Ni}(\mu\text{-OH})_2]\text{Cl}_2$ (**10**) with thermal ellipsoids drawn at the 35% probability level. The outer-sphere chloride, hydrogen atoms attached to carbon, phenyl groups, and co-crystallized CH_2Cl_2 were omitted from the figure.

The reaction eliminated an equivalent of $[\text{Bu}_4\text{N}]\text{Cl}$, which was co-crystallized from the reaction mixtures. The structure of **10** revealed *trans* B–F and N–H bonds and an elongated dative $\text{N}\rightarrow\text{B}$ bond distance of 1.613(3) Å, which is *ca.* 0.03–0.04 Å shorter than those in **5** and **7–9** (Table 2). The B–F distances of 1.415(3) and 1.424(3) Å are similar to the B–OH distance in **5** of 1.427(4) Å, but slightly longer than those observed in the $\text{N}_3\text{B-F}$ core of subporphyrin complexes (1.39–1.41 Å).^{54–56} Despite the similar B–O and B–F distances, none of our data suggested that **5** and **10** were the same compound. Attempts to replace fluoride in the XRD data collected for **10** with oxygen led to unsatisfactory ellipsoids and a higher *R*-factor. ^{19}F NMR spectra collected on crystallized samples of **10** yielded a broad resonance at δ –164.5 in CDCl_3 . The ^{19}F NMR shift for **10** is similar to those in the aforementioned fluorinated subporphyrin complexes, which range between δ –156 and –158.^{54,55} For added comparison, the ^{19}F NMR resonance for the $[\text{Bu}_4\text{N}]\text{F}$ starting material appears at δ –125.7 in CDCl_3 .⁵⁷ The ^{11}B and ^{31}P NMR resonances for **10** were observed at δ 1.6 and 72.0, respectively, and are slightly shifted compared to those observed for **5** in CDCl_3 at δ 1.0 and 70.8 (Table 1). No ^{11}B – ^{19}F coupling was observed, as is typical for some $\text{O}\rightarrow\text{B}$ and $\text{N}\rightarrow\text{B}$ dative complexes containing B–F bonds (*e.g.*, $\text{BF}_3\cdot\text{Et}_2\text{O}$ and $\text{BF}_3\cdot\text{MeCN}$),⁵⁸ but the ^{11}B resonance for **10** (FWHM = 180 Hz) was significantly broadened compared to **5** (FWHM = 80 Hz). The ^1H NMR spectrum of **10** corroborated the determined structure in Fig. 12 and revealed no resonances assigned to B–OH (Fig. S49; ESI[†]). Moreover, acquisition of the NMR data for **10** did not require addition of NEt_3 , nor was any HF loss or decomposition observed.

Conclusion

In summary, we have reported two new triaminoborane-bridged diphosphine ligands, $^{\text{Ph}}\text{TBDPhos}$ and $^{\text{iPr}}\text{TBDPhos}$, and established their coordination chemistry with NiCl_2 and PdCl_2 . The bridgehead B–N bond in $^{\text{Ph}}\text{TBDPhos}$ selectively reacts with water, alcohols, and fluoride when bound to $\text{Ni}(\text{II})$ (**1**) and $\text{Pd}(\text{II})$ (**3**), whereas the $^{\text{iPr}}\text{TBDPhos}$ complexes **2** and **4**

show no appreciable reactivity. The lack of $^{\text{iPr}}\text{TBDPhos}$ reactivity is attributed to the sterically bulky isopropyl groups, which block substrate access to boron in the TBD backbone. The reactivity studies suggest that protonation of the bridgehead nitrogen in $^{\text{Ph}}\text{TBDPhos}$ helps to overcome the lack of measurable Lewis acidity at boron, an observation supported by methoxide and fluoride binding studies with TASF and hydrated $[\text{Bu}_4\text{N}]\text{F}$. Furthermore, when H_2O and alcohol reaction products **5–9** are dissolved in anhydrous solvent, especially without addition of NEt_3 , the compounds revert back to some proportion of starting materials **1** and **3**. As described in a recent review by Maity and Teets,¹⁴ irreversible B–O formation is a long-standing challenge when using borane ligands in catalytic and stoichiometric reactions. Our results hint at reversible B–O reactivity, but more work is needed to account for the small amounts of $^{\text{Ph}}\text{TBDPhos}$ decomposition.

Returning to Chart 1 in the introduction, we noted that triaminoboranes participating in Z-type $\text{M}\rightarrow\text{B}$ σ bonds can promote cooperative metal–ligand reactivity. By way of analogy, our results suggest that dative $\text{N}\rightarrow\text{B}$ π bonds in $^{\text{Ph}}\text{TBDPhos}$ can promote reactions without obvious participation of the metal. Given that participation of the bridgehead nitrogen in TBDPhos appears to be important for promoting reactivity at boron, we propose to define these types of reactions (*i.e.*, chemical reactions requiring more than one atom on a ligand) as “cooperative ligand-centered reactivity” (CLR). Our rationale for defining CLR here is two-fold: (1) to distinguish the reactivity from cooperative metal–ligand reactions and ligand-centered reactivity involving a single atom on the ligand (*e.g.*, Lewis acid or base binding), and (2) to highlight it as a potential ligand design principle.

Li and Hall recently proposed a catalytic cycle that proceeds *via* concerted transfer of two hydrogen atoms on MeOH to carbon and nitrogen atoms on a Ru-bound ligand in a “ligand–ligand bifunctional mechanism”.⁵⁹ We chose to use “cooperative” in defining CLR instead of “bifunctional” because bifunctional has been used historically to imply concerted reactivity across metal–ligand bonds in metal–ligand bifunctional catalysts. Dub and Gordon recently proposed that the long-entrenched view of concerted reactivity is incorrect in Noyori’s archetypal catalysts and, in turn, offered an expanded description of metal–ligand cooperativity (MLC) to more adequately define cooperative ligands:^{60,61}

“Therefore in order for the principle of metal–ligand cooperativity to take place, a ligand should act together in a synergistic manner with the metal to facilitate a chemical event, *i.e.*, any act of bond cleavage/formation...ligands defined in such a way can be called cooperative”.⁶⁰

Notably, reactions captured in the expanded description can proceed *via* concerted or step-wise reaction steps. Hence, we submit that “cooperative”, as used in Dub and Gordon’s definition of MLC, provides a less restrictive qualifier to define ligand-centered reactions involving more than one atom, such as those described here. Future work is aimed at elucidating the mechanism of $^{\text{Ph}}\text{TBDPhos}$ reactivity and exploring the applications of these and other CLR-type reactions.

Experimental

General considerations

Reactions were carried out under an atmosphere of N₂ or Ar using glovebox or standard Schlenk techniques unless stated otherwise. Glassware used for reactions performed under inert conditions were dried in an oven at 150 °C for at least 1.5 h and allowed to cool under vacuum before use. Solvents used for anhydrous reactions were dried and deoxygenated using a Pure Process Technologies Solvent Purification System. NaBH₄, I₂, 3,3'-diaminodipropylamine, ClPPh₂, ClPⁱPr₂, ⁿBuLi (2.5 M in hexanes), (DME)NiCl₂, (PhCN)₂PdCl₂, MeOH, allylic alcohol, [ⁿBu₄N]F·(H₂O)_n, tris(dimethylamino)sulfonium difluorotrimethylsilicate (TASF), NaOMe, and ampules of deuterated solvents were used as received from commercial vendors. NEt₃ was dried over KOH and distilled before use.

¹H, ¹⁹F, and ³¹P NMR data were recorded on a Bruker AVANCE-300 instrument operating at 300 MHz for ¹H, 282.2 MHz for ¹⁹F, and 121.4 MHz for ³¹P. ¹¹B and ¹³C NMR data were acquired on a Bruker DRX-400 instrument operating at 128.3 and 75.5 MHz, respectively. Chemical shifts are reported in δ units relative to residual solvent peaks (¹H and ¹³C), 0.05% C₆H₅CF₃ in C₆D₆ (¹⁹F), 85% H₃PO₄ (³¹P), and BF₃·Et₂O (¹¹B). Microanalysis data (CHN) were collected using an EAI CE-440 Elemental Analyzer at the University of Iowa or by Midwest Microlab, LLC in Indianapolis, IN. IR spectra were collected on a Thermo Scientific Nicolet iS5 using an attenuated total reflection (ATR) accessory, as KBr pellets, or as Nujol mulls between NaCl plates. Melting points were determined using a REACH MP Device. HR-EI mass spectra were recorded on Waters GCT Premier instrument using TOF, and ESI-MS spectra were collected on Waters Q-TOF premier. Fragment ions (M: molecule, L: ligand) were assigned based on comparison to calculated natural abundance isotopic distributions.

1,8,10,9-Triazaboradecalin (TBD)

Prepared with slight modification to a published procedure.⁴¹ To a suspension of NaBH₄ (4.30 g, 0.114 mol) and 3,3'-diaminodipropylamine (13.1 g, 0.100 mol) in THF (200 mL) was added a solution of I₂ (12.7 g, 0.0500 mol) in THF (100 mL). The mixture was heated to reflux for 3 days. After cooling to RT, the solution was filtered. The solvent was removed under vacuum and the residue was distilled under vacuum. The distillate was heated at 150 °C overnight to complete the reaction. The resulting solid was dissolved in pentane (20 mL), filtered, and stored at -30 °C to yield colorless needles. Yield: 7.68 g (55%). The purity and identity of TBD were confirmed by ¹H and ¹¹B NMR spectroscopy. ¹H NMR (CDCl₃, 20 °C): δ 1.69 (br s, NH, 2H), 1.79 (quint, CH₂-CH₂-CH₂, 4H), 2.84 (vt, NCH₂, 4H), 2.98 (vt, NCH₂, 4H). ¹¹B NMR (CDCl₃, 20 °C): δ 22.4 (s).

^{Ph}TBDPhos

A solution of ClPPh₂ (6.40 g, 29.0 mmol) in CH₂Cl₂ (40 mL) was slowly added to a solution of TBD (2.00 g, 14.4 mmol) and NEt₃ (2.92 g, 28.9 mmol) in CH₂Cl₂ (40 mL). The reaction

mixture was stirred overnight and the solvent was removed under vacuum. The solid residue was extracted with Et₂O (3 × 100 mL), filtered, and the filtrate was evaporated to dryness under vacuum. The resulting white solid was dissolved in CH₂Cl₂ (15 mL), concentrated, and cooled to -30 °C to yield colorless blocks after 1 day. Yield: 7.00 g (96%). Mp: 167 °C. Anal. calcd for C₃₀H₃₂BN₃P₂: C, 71.0; H, 6.36; N, 8.28. Found: C, 70.4; H, 6.12; N, 8.30. ¹H NMR (CDCl₃, 20 °C): δ 1.37 (quint, CH₂-CH₂-CH₂, 4H), 2.80 (t, NCH₂, 4H), 3.05 (m, NCH₂, 4H), 7.30–7.40 (m, Ph, 12H), 7.51–7.55 (m, Ph, 8H). ¹¹B NMR (CDCl₃, 20 °C): δ 26.2 (br s, FWHM = 580 Hz). ¹³C NMR (CDCl₃, 20 °C): δ 27.3 (s, CH₂-CH₂-CH₂), 44.3 (s, NCH₂), 48.4 (s, NCH₂), 127.7 (vt, Ph, ³J_{PC} = 2.7 Hz), 127.8 (s, Ph), 132.9 (vt, Ph, ¹J_{PC} = 11.0 Hz), 139.7 (vt, Ph, ²J_{PC} = 8.0 Hz). ³¹P{¹H} NMR (CDCl₃, 20 °C): δ 47.7 (s). MS (FI) [fragment ion, relative abundance]: *m/z* 108 [PPh, 12], 183 [PPh₂, 31], 322 [L - PPh₂, 18], 430 [L - Ph, 100], 507 [L, 42]. IR (Nujol, cm⁻¹): 1582 w, 1501 m, 1348 vw, 1316 vw, 1298 w, 1286 w, 1274 vw, 1205 s, 1170 m, 1110 s, 1095 w, 1067w, 1022 s, 997 m, 984 vw, 964 m, 930 w, 919 w, 878 s, 847 w, 814 s, 772 m, 746 vs, 724 w, 700 vs, 656 vw, 648 m, 634 m, 617 vw, 578 vw.

^{iPr}TBDPhos

To a stirring solution of TBD (2.00 g, 14.4 mmol) in Et₂O (50 mL) cooled to -78 °C was added a solution of 2.5 M ⁿBuLi in hexanes (11.5 mL, 28.8 mmol). The white suspension was stirred for a day. A solution of ClPⁱPr₂ (5.20 g, 28.8 mmol) in Et₂O (50 mL) was added and the reaction mixture was stirred for 5 days. The solvent was removed under vacuum and the solid residue was extracted with Et₂O (3 × 100 mL) and filtered. The filtrate was evaporated to dryness under vacuum and the resulting white solid was dissolved in CH₂Cl₂ (10 mL), concentrated, and stored at -30 °C to yield colorless blocks. Yield: 1.77 g (33%). Mp: 70 °C. Anal. calcd for C₁₈H₄₀BN₃P₂: C, 58.2; H, 10.9; N, 11.3. Found: C, 58.0; H, 10.8; N, 11.2. ¹H NMR (CDCl₃, 20 °C): δ 1.00–1.15 (m, CH₃-CH-CH₃, 24 H), 1.72 (quint, -CH₂-CH₂-CH₂-, 4 H), 1.87 (sept, CH₃-CH-CH₃, 4 H), 2.84 (t, NCH₂, 4 H), 2.95 (m, NCH₂, 4 H). ¹¹B NMR (CDCl₃, 20 °C): δ 25.8 (br s, FWHM = 200 Hz). ¹³C NMR (CDCl₃, 20 °C): δ 20.2 (vt, CH₃-CH-CH₃, ¹J_{PC} = 14.4 Hz), 21.0 (vt, CH₃-CH-CH₃, ²J_{PC} = 8.9 Hz), 26.1 (vt, CH₃-CH-CH₃, ²J_{PC} = 8.9 Hz), 28.0 (s, CH₂-CH₂-CH₂), 43.1 (s, NCH₂), 48.9 (s, NCH₂). ³¹P{¹H} NMR (CDCl₃, 20 °C): δ 61.3 (s). MS (FI) [fragment ion, relative abundance]: *m/z* 200 [M - ⁴iPr, 9], 242 [M - ³iPr, 9], 285 [M - ²iPr, 29], 328 [M - ¹iPr, 100], 371 [M, 5]. IR (Nujol, cm⁻¹): 1500 s, 1356 vw, 1347 vw, 1315 s, 1290 s, 1236 vw, 1211 s, 1182 m, 1153 w, 1115 s, 1068 m, 1024 s, 966 s, 927 m, 875 s, 817 s, 777 m, 764 m, 749 m, 722 m, 639 s, 598 w.

(^{Ph}TBDPhos)NiCl₂ (1)

To a solution of (DME)NiCl₂ (0.10 g, 0.46 mmol) in CH₂Cl₂ (10 mL) was added a solution of ^{Ph}TBDPhos (0.23 g, 0.45 mmol) in CH₂Cl₂ (10 mL). After 30 min, the color of the reaction mixture changed from yellow to dark orange. The mixture was evaporated to dryness under vacuum and extracted with CH₂Cl₂ (10 mL). Vapor diffusion with Et₂O

yielded orange needles and dark orange blocks that were determined to be polymorphs of **1**. Yield: 0.23 g (79%). Mp: >250 °C. Anal. calcd for $C_{30}H_{32}BCl_2N_3NiP_2 \cdot 2CH_2Cl_2$: C, 47.6; H, 4.50; N, 5.21. Found: C, 47.8; H, 4.49; N, 5.19. 1H NMR ($CDCl_3$, 20 °C): δ 1.49 (m, $CH_2-CH_2-CH_2$, 4H), 2.72 (m, NCH₂, 4H), 2.81 (t, NCH₂, 4H), 7.37–7.53 (m, Ph, 12H), 7.85–7.99 (d, Ph, 8H). ^{11}B NMR ($CDCl_3$, 20 °C): δ 23.9 (br s, FWHM = 540 Hz). ^{13}C NMR ($CDCl_3$, 20 °C): δ 26.0 (s, $CH_2-CH_2-CH_2$), 47.3 (s, NCH₂), 48.1 (s, NCH₂), 128.4 (s, Ph), 130.8 (s, Ph), 132.9 (s, Ph). $^{31}P\{^1H\}$ NMR ($CDCl_3$, 20 °C): δ 70.1 (br s, FWHM = 140 Hz). MS (FI) [fragment ion, relative abundance]: m/z 183 [PPh₂, 10], 322 [L – PPh₂, 9], 353 [L – 2Ph, 1], 379 [M – 2Cl[−] – PPh₂, 3], 415 [M – Cl[−] – PPh₂, 6], 430 [L – Ph, 100], 446 [M – Cl[−] – 2Ph, 13], 523 [M – Cl[−] – Ph, 5], 564 [M – 2Cl, 2], 600 [M – Cl, 13], 637 [M, 1]. IR (Nujol, cm^{-1}): 1322 w, 1305 w, 1291 s, 1223 w, 1214 vw, 1206 s, 1179 s, 1170 vw, 1154 vw, 1119 vw, 1098 s, 1071 vw, 1024 s, 1009 w, 998 w, 938 m, 909 s, 891 m, 826 s, 783 s, 749 s, 724 s, 711 m, 693 s, 648 m, 629 m, 618 w, 595 m, 568 w, 535 w.

(ⁱPrTBDPhos)NiCl₂ (2)

To a stirring solution of (DME)NiCl₂ (0.30 g, 1.37 mmol) in CH₂Cl₂ (20 mL) was added a solution of ⁱPrTBDPhos (0.51 g, 1.37 mmol) in CH₂Cl₂ (10 mL). Stirring the mixture overnight yielded a dark blue solution. The solution was concentrated to ca. 10 mL and dark blue blocks were obtained by vapor diffusion with Et₂O. Yield: 0.52 g (76%). Mp: 226 °C. Anal. calcd for $C_{18}H_{40}BCl_2N_3NiP_2$: C, 43.2; H, 8.05; N, 8.39. Found: C, 42.6; H, 7.92; N, 8.07. 1H NMR ($CDCl_3$, 20 °C): δ 1.45 (d, $CH_3-CH-CH_3$, 12 H), 1.64 (d, $CH_3-CH-CH_3$, 12 H), 1.81 (quint, $-CH_2-CH_2-CH_2-$, 4 H), 2.92 (t, NCH₂, 4 H), 3.16 (sept, $CH_3-CH-CH_3$, 4 H), 3.21 (m, NCH₂, 4 H). ^{11}B NMR ($CDCl_3$, 20 °C): δ 24.5 (br s, FWHM = 320 Hz). ^{13}C NMR ($CDCl_3$, 20 °C): δ 19.4 (s, $CH_3-CH-CH_3$), 19.6 (s, $CH_3-CH-CH_3$), 27.1 (s, $CH_3-CH-CH_3$ or $CH_2-CH_2-CH_2$), 28.3 (s, $CH_2-CH_2-CH_2$ or $CH_3-CH-CH_3$), 45.4 (s, NCH₂), 48.4 (s, NCH₂). $^{31}P\{^1H\}$ NMR ($CDCl_3$, 20 °C): δ 147.7 (br s, FWHM = 1200 Hz). MS (FI) [fragment ion, relative abundance]: m/z 200 [L – ⁱPr, 72], 242 [L – ³Pr, 65], 254 [M – 2Cl – ⁱPr, 67], 285 [L – ²Pr, 78], 298 [M – 2Cl – ³Pr, 100], 328 [L – ⁱPr, 84], 342 [M – 2Cl – ²Pr, 65], 384 [M – 2Cl – ⁱPr, 34], 466 [M – Cl, 98], 501 [M, 2]. IR (Nujol, cm^{-1}): 1526 w, 1514 s, 1327 m, 1303 w, 1292 w, 1277 m, 1241 m, 1212 s, 1161 s, 1101 m, 1079 vw, 1064 vw, 1042 s, 1008 w, 968 m, 938 w, 900 m, 879 m, 846 w, 819 m, 765 m, 722 vs, 655 m, 623 m.

(^{Ph}TBDPhos)PdCl₂ (3)

To a stirring solution of (PhCN)₂PdCl₂ (0.20 g, 0.52 mmol) in toluene (10 mL) was added a solution of ^{Ph}TBDPhos (0.26 g, 0.52 mmol) in toluene (10 mL). A dark brown precipitate formed and the mixture was stirred overnight. The precipitate was filtered and evaporated to dryness under vacuum. Yield: 0.27 g (75%). Brown needles and blocks were subsequently obtained by vapor diffusion of Et₂O into CH₂Cl₂ solutions of **3**. Mp: 198 °C (dec). Anal. calcd for $C_{30}H_{32}BCl_2N_3P_2Pd \cdot 2CH_2Cl_2$: C, 45.0; H, 4.25; N, 4.92. Found: C, 45.0; H, 4.17; N, 4.91. 1H NMR ($CDCl_3$, 20 °C): δ 1.56 (quint, $-CH_2-CH_2-CH_2-$, 4 H),

2.81–2.97 (m, NCH₂, 8 H), 7.34–7.50 (m, Ph, 12 H), 7.72–7.84 (m, Ph, 8 H). ^{11}B NMR ($CDCl_3$, 20 °C): δ 24.2 (br s, FWHM = 440 Hz). ^{13}C NMR ($CDCl_3$, 20 °C): δ 26.2 (s, $CH_2-CH_2-CH_2$), 47.5 (s, NCH₂), 48.3 (s, NCH₂), 128.5 (m, Ph), 130.2 (s, Ph), 131.3 (s, Ph), 133.0 (m, Ph). $^{31}P\{^1H\}$ NMR ($CDCl_3$, 20 °C): δ 68.7 (s). MS (FI) [fragment ion, relative abundance]: 183 [PPh₂, 83], 430 [L – Ph, 100], 507 [L, 14], 535 [M – 2Cl – Ph, 1], 613 [M – 2Cl, 4], 648 [M – Cl, 2]. IR (Nujol, cm^{-1}): 1395 m, 1298 m, 1281 m, 1269 w, 1257 w, 1211 s, 1172 s, 1157 w, 1119 w, 1093 s, 1056 w, 1026 s, 1010 w, 997 w, 918 s, 892 s, 834 m, 786 m, 742 m, 723 s, 691 s, 638 w, 617 w, 601 w.

(ⁱPrTBDPhos)PdCl₂ (4)

To a stirring solution of (PhCN)₂PdCl₂ (0.30 g, 0.782 mmol) in toluene (10 mL) was added a solution of ⁱPrTBDPhos (0.29 g, 0.781 mmol) in toluene (10 mL). The reaction mixture was stirred overnight, filtered, and evaporated to dryness under vacuum. The resulting pale yellow powder was dissolved in CH₂Cl₂ (5 mL) and filtered. Colorless blocks were obtained by vapor diffusion with Et₂O. Yield: 0.30 g (70%). Mp 142 °C (dec). Anal. calcd for $C_{18}H_{40}BCl_2N_3P_2Pd$: C, 39.4; H, 7.35; N, 7.66. Found: C, 39.1; H, 7.29; N, 7.52. 1H NMR ($CDCl_3$, 20 °C): δ 1.32–1.54 (m, $CH_3-CH-CH_3$, 24 H), 1.83 (quint, $-CH_2-CH_2-CH_2-$, 4 H), 2.94 (t, NCH₂, 4 H), 3.19–3.37 (m, NCH₂, $CH_3-CH-CH_3$, 8 H). ^{11}B NMR ($CDCl_3$, 20 °C): δ 24.5 (br s, FWHM = 320 Hz). ^{13}C NMR ($CDCl_3$, 20 °C): δ 19.6 (s, $CH_3-CH-CH_3$), 20.4 (s, $CH_3-CH-CH_3$), 26.9 (s, $CH_2-CH_2-CH_2$), 29.9 (d, $CH_3-CH-CH_3$, $^1J_{PC} = 2.6$ Hz), 30.3 (d, $CH_3-CH-CH_3$, $^1J_{PC} = 2.7$ Hz), 45.8 (s, NCH₂), 48.9 (s, NCH₂). $^{31}P\{^1H\}$ NMR ($CDCl_3$, 20 °C): δ 97.4 (s). MS (FI) [fragment ion, relative abundance]: m/z 305 [M – 2Cl – ⁱPr, 100], 348 [M – 2Cl – ³Pr, 64], 391 [M – 2Cl – ²Pr, 50], 434 [M – 2Cl – ⁱPr, 53], 477 [M – 2Cl, 63], 512 [M – Cl, 66]. IR (Nujol, cm^{-1}): 1508 s, 1354 w, 1324 m, 1296 m, 1284 vw, 1263 m, 1225 w, 1211 vw, 1202 s, 1173 s, 1121 w, 1094 s, 1054 m, 1022 s, 1011 vw, 966 w, 943 m, 913 m, 897 m, 886 m, 822 s, 781 s, 722 s, 656 s, 635 w, 613 m.

{[(^{Ph}TBDPhos-H₂O)Ni]₂(μ -OH)₂}Cl₂ (5)

To a solution of **1** (0.20 g, 0.31 mmol) in CHCl₃ (10 mL) in air was added NEt₃ (0.5 mL) and deionized H₂O (5 mL). A single agitation of the solution completed the reaction as indicated by a color change from dark to bright orange and subsequent ^{11}B and ^{31}P NMR analysis of the reaction mixture. The CHCl₃ fraction was separated from the water layer and pentane was added to precipitate a yellow-orange powder. Yield: 0.10 g (50%). Single crystals were obtained by layering of the CHCl₃ solution with hexane. Anal. calcd for $C_{60}H_{70}B_2Cl_2N_6Ni_2O_4P_4$: C, 56.6; H, 5.54; N, 6.60. Found: C, 56.1; H, 5.79; N, 6.34. 1H NMR ($CDCl_3$, 20 °C): δ −4.48 (s, 1H, Ni-OH), 0.25 (s, 1H, B-OH), 1.04 (m, 2H), 1.89 (m, 2H), 2.64 (br s, 2H), 2.73 (m, 2H), 2.94 (m, 2H), 3.26 (m, 2H), 7.11–7.22 (m, 6H, Ph), 7.38–7.51 (m, 10H, Ph), 7.66 (m, 4H, Ph), 8.44 (m, 1H, NH). ^{11}B NMR ($CDCl_3$, 20 °C): δ 1.0 (s). ^{13}C NMR ($CDCl_3$, 20 °C): δ 26.4 (s, $CH_2-CH_2-CH_2$), 45.9 (s, NCH₂), 49.4 (s, NCH₂), 128.9 (m, Ph), 129.0 (vt, Ph, $J_{PC} = 5.1$ Hz), 130.6 (d, Ph, $J_{PC} = 9.2$ Hz), 131.6 (vt, Ph, $J_{PC} = 5.5$ Hz), 132.1 (m, Ph), 133.2 (vt, Ph,

$J_{\text{PC}} = 5.0 \text{ Hz}$). $^{31}\text{P}\{^1\text{H}\}$ NMR (CDCl_3 , 20°C): δ 70.8 (s). MS (FI) [fragment ion, relative abundance]: m/z 353 [TBDPhos – 2Ph, 12], 591 [(M – H₂O – 2HCl)²⁺, 22], 600 [(TBDPhos)Ni(OH)₂, 100], 618 [M – (^{Ph}TBDPhos-H₂O)Ni²⁺, 70], 676 [M – ^{Ph}TBDPhos-H₂O, 23], 1237 [M – Cl⁻, 23]. IR (KBr, cm^{-1}): 3630 s (Ni–OH), 3372 br (B–OH), 3048 w, 3012 m, 2937 w, 2857 m, 1483 m, 1436 s, 1388 m, 1369 m, 1352 w, 1298 m, 1261 m, 1242 m, 1220 w, 1165 m, 1092 vs, 1047 s, 1027 w, 1003 m, 977 w, 912 m, 880 s, 836 w, 801 vw, 778 w, 756 m, 745 m, 710 vw, 697 s, 637 m, 561 m, 527 m, 507 w, 489 m.

$\{[(^{\text{Ph}}\text{TBDPhos-H}_2\text{O})\text{Pd}]_2(\mu\text{-OH})_2\}\text{Cl}_2$ (6)

A mixture of **3** (0.10 g, 0.14 mmol) and NEt_3 (0.5 mL) was dissolved in CH_2Cl_2 (10 mL) in air. The pale-yellow solution was layered with deionized H_2O (10 mL) and stirred vigorously for 30 min. The CH_2Cl_2 layer was separated and filtered. Addition of pentane (10 mL) precipitated a pale yellow powder. Yield: 0.026 g (26%). Anal. calcd for $\text{C}_{60}\text{H}_{70}\text{B}_2\text{Cl}_2\text{N}_6\text{O}_4\text{P}_4\text{Pd}_2$: C, 52.7; H, 5.16; N, 6.14. Found: C, 52.1; H, 5.10; N, 5.82. ^1H NMR (CD_2Cl_2 , 20°C): δ –2.89 (s, 1H, Pd–OH), 0.87 (s, 1H, B–OH), 1.10 (m, 2H), 1.91 (m, 2H), 2.65 (m, 2H), 2.90 (m, 4H), 3.47 (m, 2H), 7.20 (m, 6H, Ph), 7.36 (m, 10H, Ph), 7.68 (m, 4H, Ph), 8.58 (br s, 1H, NH). ^{11}B NMR (CD_2Cl_2 , 20°C): δ 1.8 (s). ^{13}C NMR (CD_2Cl_2 , 20°C): δ 26.7 (s, $\text{CH}_2\text{-CH}_2\text{-CH}_2$), 46.4 (s, NCH₂), 49.6 (s, NCH₂), 129.0 (m, Ph), 131.0 (s, Ph), 131.2 (s, Ph), 131.6 (s, Ph), 132.2 (m, Ph), 133.2 (m, Ph), 133.5 (m, Ph). $^{31}\text{P}\{^1\text{H}\}$ NMR (CD_2Cl_2 , 20°C): δ 65.3 (s). IR (ATR, cm^{-1}): 3607 m (Pd–OH), 3340 br (B–OH), 3049 m, 2940 m, 2856 m, 1586 w, 1481 w, 1456 w, 1434 s, 1373 m, 1297 m, 1260 w, 1240 m, 1148 w, 1121 w, 1097 s, 1044 s, 1025 w, 997 w, 921 w, 884 sm, 833 w, 744 s, 711 w, 693 vs, 634 s, 619 w, 590 w, 583 w, 574 w, 567 w, 554 m.

$(^{\text{Ph}}\text{TBDPhos-MeOH})\text{NiCl}_2$ (7)

To a mixture of **1** (0.20 g, 0.31 mmol) and NEt_3 (0.5 mL) was added MeOH (10 mL) in air. The mixture was stirred for 20 min until everything dissolved. ^{11}B and ^{31}P NMR analysis of the resulting light orange solution revealed that the reaction was complete. Vapor diffusion of Et_2O into the solution yielded orange blocks after 3 days. Yield: 0.10 g (49%). Anal. calcd for $\text{C}_{31}\text{H}_{36}\text{BCl}_2\text{N}_3\text{NiOP}_2\text{-CH}_3\text{OH}$: C, 54.8; H, 5.75; N, 5.99. Found: C, 54.8; H, 5.64; N, 6.32. ^1H NMR (CDCl_3 , 20°C): δ 0.97 (d, 2H), 1.85 (m, 2H), 2.59 (br s, 2H), 2.62 (s, 3H, MeO), 2.71 (m, 2H), 2.87 (m, 2H), 3.02 (m, 2H), 7.03 (m, 4H), 7.11 (m, 2H), 7.42 (m, 2H), 7.51 (m, 4H), 7.67 (m, 4H), 7.92 (m, 4H), 8.49 (m, 1H, NH). ^{11}B NMR (CDCl_3 , 20°C): δ 1.9 (s). ^{13}C NMR (CDCl_3 , 20°C): δ 26.2 (s, $\text{CH}_2\text{-CH}_2\text{-CH}_2$), 46.4 (s, OCH₃), 47.9 (s, NCH₂), 49.3 (s, NCH₂), 128.7 (m, Ph), 130.2 (s, Ph), 130.8 (m, Ph), 132.6 (m, Ph), 133.3 (m, Ph). $^{31}\text{P}\{^1\text{H}\}$ NMR (CDCl_3 , 20°C): δ 69.8 (s). MS (FI) [fragment ion, relative abundance]: m/z 78 [Ph, 100], 600 [M – Cl⁻ – CH₃OH, 3]. IR (KBr, cm^{-1}): 3199 m, 3056 w, 2943 m, 2866 m, 2808 m, 1479 m, 1459 vw, 1448 w, 1432 s, 1400 w, 1369 m, 1351 m, 1292 m, 1244 m, 1191 m, 1132 m, 1099 vs, 1039 vs, 999 w, 978 w, 941 w, 912 m, 870 s, 828 w, 794 m, 756 m, 746 m, 695 vs, 622 w, 609 s, 564 w, 551 w, 541 w, 530 w, 502 m, 483 w.

$(^{\text{Ph}}\text{TBDPhos-MeOH})\text{PdCl}_2$ (8)

To a mixture of **3** (0.10 g, 0.14 mmol) and NEt_3 (0.5 mL) was added a 1 : 1 mixture of CH_2Cl_2 and MeOH (15 mL) in air. The orange-yellow solution was stirred for 10 min, filtered, and concentrated to ca. 2 mL. Single crystal were obtained by vapor diffusion with Et_2O . Yield: 0.065 g (62%). Anal. calcd for $\text{C}_{31}\text{H}_{36}\text{BCl}_2\text{N}_3\text{OP}_2\text{Pd}$: C, 51.9; H, 5.06; N, 5.86. Found: C, 51.6; H, 5.34; N, 6.25. ^1H NMR (DMSO-d_6 , 20°C): δ 1.24 (m, 4H), 2.54–2.81 (m, 9H), 2.91 (m, 2H), 5.85 (s, 1H, NH), 7.50 (m, 12H), 7.94 (m, 8H). ^{11}B NMR (DMSO-d_6 , 20°C): δ 3.2 (s). ^{13}C NMR (DMSO-d_6 , 20°C): δ 25.3 (s, $\text{CH}_2\text{-CH}_2\text{-CH}_2$), 45.9 (s, OCH₃), 47.6 (s, NCH₂), 48.9 (s, NCH₂), 127.6 (m, Ph), 128.5 (m, Ph), 130.1 (d, Ph, $J_{\text{PC}} = 20.0 \text{ Hz}$), 130.6 (d, Ph, $J_{\text{PC}} = 14.7 \text{ Hz}$), 131.2 (s, Ph), 132.6 (m, Ph), 133.1 (m, Ph), 133.6 (m, Ph), 134.2 (s, Ph). $^{31}\text{P}\{^1\text{H}\}$ NMR (DMSO-d_6 , 20°C): δ 64.5 (s). IR (ATR, cm^{-1}): 3189 m, 3043 w, 2975 m, 2941 m, 2909 w, 2867 m, 2807 m, 1569 w, 1478 m, 1447 w, 1431 s, 1399 w, 1368 m, 1352 m, 1292 m, 1243 s, 1189 s, 1157 w, 1132 s, 1108 w, 1088 vs, 1037 vs, 1023 w, 999 w, 972 w, 942 m, 912 s, 870 vs, 827 m, 792 s, 755 s, 745 s, 693 vs, 622 m, 610 s, 599 w, 590 w, 579 m.

$(^{\text{Ph}}\text{TBDPhos-C}_3\text{H}_5\text{OH})\text{PdCl}_2$ (9)

A mixture of **3** (0.10 g, 0.14 mmol) and NEt_3 (0.5 mL) was dissolved in 15 mL solvent mixture of CH_2Cl_2 and allyl alcohol (1 : 1) in air. The green-yellow solution was stirred for 10 min, filtered, and concentrated to ca. 2 mL. Single crystals were obtained by vapor diffusion with Et_2O . Yield: 0.086 g (80%). Anal. calcd for $\text{C}_{33}\text{H}_{38}\text{BCl}_2\text{N}_3\text{OP}_2\text{Pd}$: C, 53.4; H, 5.16; N, 5.66. Found: C, 53.1; H, 5.40; N, 5.87. ^1H NMR (CD_2Cl_2 , 20°C): δ 1.29 (m, 4H), 2.74 (m, 2H), 3.04 (m, 6H), 3.38 (m, 2H), 4.90–5.09 (m, 2H), 5.66–5.80 (m, 1H), 7.42–7.59 (m, 13H), 7.89–8.04 (m, 8H). ^{11}B NMR (CD_2Cl_2 , 20°C): δ 2.9 (s). ^{13}C NMR (CD_2Cl_2 , 20°C): δ 26.8 (s, $\text{CH}_2\text{-CH}_2\text{-CH}_2$), 46.4 (s, NCH₂), 50.3 (s, NCH₂), 60.9 (s, BOCH₂), 112.8 (s, $-\text{CH}=\text{CH}_2$), 128.5 (m, Ph), 131.0 (s, Ph), 131.3 (s, Ph), 131.6 (s, Ph), 133.3 (m, Ph), 134.3 (m, Ph), 134.9 (s, Ph), 138.6 (s, $-\text{CH}=\text{CH}_2$). $^{31}\text{P}\{^1\text{H}\}$ NMR (CD_2Cl_2 , 20°C): δ 66.1 (s). IR (ATR, cm^{-1}): 3203 m, 3054 w, 2980 m, 2918 w, 2865 w, 2828 m, 1568 w, 1478 m, 1447 w, 1431 s, 1398 w, 1369 m, 1348 m, 1293 m, 1244 m, 1190 m, 1165 m, 1128 s, 1108 w, 1084 vs, 1037 vs, 1024 w, 998 w, 986 w, 949 m, 917 s, 875 vs, 828 m, 786 s, 748 s, 740 w, 694 vs, 623 w, 605 s, 585 w, 577 w, 572 w.

$\{[(^{\text{Ph}}\text{TBDPhos-HF})\text{Ni}]_2(\mu\text{-OH})_2\}\text{Cl}_2$ (10)

To a solution of **1** (0.10 g, 0.16 mmol) in CH_2Cl_2 (10 mL) was added a solution of 1 M [ⁿBu₄N]F·(H₂O)_n in THF (0.16 mL, 0.16 mmol). The solution immediately transformed from dark orange to orange-yellow. After stirring for 1 h, the reaction was evaporated to dryness, dissolved in CH_2Cl_2 (5 mL), and filtered. Vapor diffusion with Et_2O yielded orange blocks with small amounts of co-crystallized [ⁿBu₄N]Cl. The crystals were dissolved in 3 mL CH_2Cl_2 and recrystallized with Et_2O to yield deep orange blocks free of [ⁿBu₄N]Cl. Yield: 0.10 g (88%). Anal. calcd for $\text{C}_{60}\text{H}_{68}\text{B}_2\text{Cl}_2\text{F}_2\text{N}_6\text{Ni}_2\text{O}_2\text{P}_4\text{-2CH}_2\text{Cl}_2$: C, 51.5; H, 5.01; N, 5.80. Found: C, 51.7; H, 4.88; N, 5.89. ^1H NMR (CDCl_3 , 20°C):

δ -4.51 (s, 1H, Ni-OH), 1.06 (m, 2H), 1.85 (m, 2H), 2.40 (br, s, 2H), 2.67 (m, 2H), 3.02 (m, 2H), 3.15 (m, 2H), 7.14–7.27 (m, 6H, Ph), 7.27–7.45 (m, 10H, Ph), 7.68 (m, 4H, Ph), 8.79 (m, 1H, NH). ^{11}B NMR (CDCl_3 , 20 °C): δ 1.6 (s). ^{13}C NMR (CDCl_3 , 20 °C): δ 26.1 (s, $\text{CH}_2\text{-CH}_2\text{-CH}_2$), 45.3 (s, NCH_2), 49.7 (s, NCH_2), 129.0 (m, Ph), 130.7 (s, Ph), 130.8 (s, Ph), 131.5 (vt, Ph), $J_{\text{PC}} = 5.5$ Hz), 133.3 (vt, Ph, $J_{\text{PC}} = 5.0$ Hz). ^{19}F NMR (CDCl_3 , 20 °C): δ -164.5 (br s, FWHM = 130 Hz). $^{31}\text{P}\{^1\text{H}\}$ NMR (CDCl_3 , 20 °C): δ 72.0 (s). IR (ATR, cm^{-1}): 3627 m (Ni-OH), 3049 w, 3003 w, 2956 m, 2884 vw, 2805 m, 2681 vw, 2644 w, 2598 vw, 2570 w, 2536 w, 1586 w, 1481 vw, 1472 w, 1459 vw, 1431 s, 1397 m, 1389 w, 1372 w, 1355 w, 1341 w, 1301 m, 1269 m, 1245 m, 1226 w, 1199 m, 1151 s, 1124 vs, 1092 vs, 1049 vs, 1028 w, 994 m, 953 m, 908 s, 884 s, 854 vw, 839 m, 810 s, 795 vw, 755 w, 746 s, 693 vs, 634 s, 614 w.

Reaction of 1 with TASF

To a stirring solution of **1** (0.10 g, 0.16 mmol) in CH_2Cl_2 (8 mL) was added a solution of dry TASF (0.045 g, 0.16 mmol) in CH_2Cl_2 (2 mL). The reaction mixture transformed from dark orange to orange-yellow over 1 day. Analysis by ^{11}B NMR spectroscopy revealed a mixture of products (δ 23.8 and 1.6; Fig. 11).

The reaction was repeated with TASF that was exposed to humidity in ambient air. ^{11}B NMR data collected revealed that the reaction converged to a single species at δ 1.6 (Fig. 11). Subsequent NMR and IR analysis of the isolated compound confirmed the formation of **10**.

Reaction of 1 with NaOMe

To a stirring suspension of NaOMe (0.025 g, 0.46 mmol) in CH_2Cl_2 (5 mL) was added a solution of **1** (0.10 g, 0.16 mmol) in CH_2Cl_2 (10 mL). The reaction revealed no visible change over the course of 2 days, which was subsequently confirmed by ^{11}B NMR spectroscopy. Only a single broad resonance was observed at δ 23.4.

Reaction of 5 with $[\text{HNET}_3]\text{Cl}$

$[\text{HNET}_3]\text{Cl}$ (0.022 g, 0.160 mmol) and **5** (0.020 g, 0.016 mmol) were dissolved in 1 mL anhydrous CDCl_3 and transferred to an NMR tube. The solution gradually changed from bright to dark orange and the reaction progress was monitored with ^{11}B and ^{31}P NMR spectroscopy until completion (48 h). ^{11}B NMR (CDCl_3 , 20 °C): δ 23.7 (br s). $^{31}\text{P}\{^1\text{H}\}$ NMR (CDCl_3 , 20 °C): δ 68.4 (s). A small peak attributed to $^{\text{Ph}}\text{TBDPhos}$ decomposition was observed at δ 27.5 in the ^{31}P NMR spectrum.

NMR analysis of 1 with $[\text{HNET}_3]\text{Cl}$

$[\text{HNET}_3]\text{Cl}$ (0.025 g, 0.182 mmol) and **1** (0.021 g, 0.033 mmol) were dissolved in 1 mL anhydrous CDCl_3 . ^{11}B NMR (CDCl_3 , 20 °C): δ 23.7 (br s). $^{31}\text{P}\{^1\text{H}\}$ NMR (CDCl_3 , 20 °C): δ 68.4 (s).

Crystallographic studies

Single crystals obtained from CH_2Cl_2 ($^{\text{Ph}}\text{TBDPhos}$ and $^{\text{iPr}}\text{TBDPhos}$), $\text{Et}_2\text{O}/\text{CH}_2\text{Cl}_2$ (**1–4**, and **10**), hexane/ CHCl_3 (**5**), $\text{Et}_2\text{O}/\text{MeOH}$ (**7**), $\text{Et}_2\text{O}/\text{CH}_2\text{Cl}_2/\text{MeOH}$ (**8**), or $\text{Et}_2\text{O}/\text{CH}_2\text{Cl}_2/\text{allyl}$

alcohol (**9**) were mounted on a MiTeGen micromount with ParatoneN oil. The data were collected as described previously.⁶² The structures were solved with Direct Methods (SHELXT or SHELXS) and least squares refinement (SHELXL) confirmed the location of the non-hydrogen atoms.⁶³ All hydrogen atom positions were idealized and were allowed to ride on the attached carbon, nitrogen or oxygen atoms. Anisotropic temperature factor for all non-hydrogen atoms were included at the last refinement. Structure solution and refinement were performed with Olex².⁶⁴ Publication figures were generated with SHELXP.⁶³ The data collection and refinement details are provided in Tables S1 and S2 (ESI†).

Acknowledgements

This work was supported by start-up funds and an Internal Funding Initiative (IFI) grant from the University of Iowa. We would like to thank Dale Swenson for collecting the single-crystal XRD data and Matthew Blake for preparing several batches of TBD.

References

- H. Braunschweig, R. D. Dewhurst and A. Schneider, *Chem. Rev.*, 2010, **110**, 3924–3957.
- H. Braunschweig and R. D. Dewhurst, *Dalton Trans.*, 2011, **40**, 549–558.
- H. Kameo and H. Nakazawa, *Chem. – Asian J.*, 2013, **8**, 1720–1734.
- G. R. Owen, *Chem. Soc. Rev.*, 2012, **41**, 3535–3546.
- G. R. Owen, *Chem. Commun.*, 2016, **52**, 10712–10726.
- G. Bouhadir and D. Bourissou, *Chem. Soc. Rev.*, 2016, **45**, 1065–1079.
- J. S. Jones and F. P. Gabbai, *Acc. Chem. Res.*, 2016, **49**, 857–867.
- C. R. Wade, A. E. J. Broomsgrove, S. Aldridge and F. P. Gabbai, *Chem. Rev.*, 2010, **110**, 3958–3984.
- C. R. Wade and F. P. Gabbai, *Inorg. Chem.*, 2010, **49**, 714–720.
- K.-N. T. Tseng, J. W. Kampf and N. K. Szymczak, *J. Am. Chem. Soc.*, 2016, **138**, 10378–10381.
- B. E. Cowie and D. J. H. Emslie, *Chem. – Eur. J.*, 2014, **20**, 16899–16912.
- B. E. Cowie and D. J. H. Emslie, *Organometallics*, 2015, **34**, 2737–2746.
- K. P. Kepp, *Inorg. Chem.*, 2016, **55**, 9461–9470.
- A. Maity and T. S. Teets, *Chem. Rev.*, 2016, **116**, 8873–8911.
- V. Gutmann, *Coord. Chem. Rev.*, 1976, **18**, 225–255.
- M. A. Beckett, G. C. Strickland, J. R. Holland and K. S. Varma, *Polymer*, 1996, **37**, 4629–4631.
- D. W. Stephan, *J. Am. Chem. Soc.*, 2015, **137**, 10018–10032.
- D. W. Stephan, *Acc. Chem. Res.*, 2015, **48**, 306–316.
- A. J. P. Cardenas, Y. Hasegawa, G. Kehr, T. H. Warren and G. Erker, *Coord. Chem. Rev.*, 2016, **306**, 468–482.
- D. W. Stephan and G. Erker, *Chem. Sci.*, 2014, **5**, 2625–2641.

- 21 L. J. Hounjet and D. W. Stephan, *Org. Process Res. Dev.*, 2014, **18**, 385–391.
- 22 D. W. Stephan, *Compr. Inorg. Chem. II*, 2013, **1**, 1069–1103.
- 23 K.-A. Ostby, A. Haaland, G. Gundersen and H. Noeth, *Organometallics*, 2005, **24**, 5318–5328.
- 24 J. S. Figueroa, J. G. Melnick and G. Parkin, *Inorg. Chem.*, 2006, **45**, 7056–7058.
- 25 V. K. Landry, J. G. Melnick, D. Buccella, K. Pang, J. C. Ulichny and G. Parkin, *Inorg. Chem.*, 2006, **45**, 2588–2597.
- 26 K. Pang, S. M. Quan and G. Parkin, *Chem. Commun.*, 2006, 5015–5017.
- 27 K. Pang, J. M. Tanski and G. Parkin, *Chem. Commun.*, 2008, 1008–1010.
- 28 A. F. Hill, G. R. Owen, A. J. P. White and D. J. Williams, *Angew. Chem., Int. Ed.*, 1999, **38**, 2759–2761.
- 29 M. R. St.-J. Foreman, A. F. Hill, G. R. Owen, A. J. P. White and D. J. Williams, *Organometallics*, 2003, **22**, 4446–4450.
- 30 N. Tsoureas, Y.-Y. Kuo, M. F. Haddow and G. R. Owen, *Chem. Commun.*, 2011, **47**, 484–486.
- 31 H. Fong, M.-E. Moret, Y. Lee and J. C. Peters, *Organometallics*, 2013, **32**, 3053–3062.
- 32 A. Zech, M. F. Haddow, H. Othman and G. R. Owen, *Organometallics*, 2012, **31**, 6753–6760.
- 33 G. R. Owen, N. Tsoureas, R. F. Hope, Y.-Y. Kuo and M. F. Haddow, *Dalton Trans.*, 2011, **40**, 5906–5915.
- 34 G. Dyson, A. Zech, B. W. Rawe, M. F. Haddow, A. Hamilton and G. R. Owen, *Organometallics*, 2011, **30**, 5844–5850.
- 35 I. R. Crossley, A. F. Hill and A. C. Willis, *Organometallics*, 2010, **29**, 326–336.
- 36 A. F. Hill, S. B. Lee, J. Park, R. Shang and A. C. Willis, *Organometallics*, 2010, **29**, 5661–5669.
- 37 Similar findings have been reported for *o*-phenylene-diamine-supported PBP pincer complexes, albeit with reactivity across B→M bonds. See: Y. Segawa, M. Yamashita and K. Nozaki, *J. Am. Chem. Soc.*, 2009, **131**, 9201–9203; M. Hasegawa, Y. Segawa, M. Yamashita and K. Nozaki, *Angew. Chem., Int. Ed.*, 2012, **51**, 6956–6960; T. Miyada and M. Yamashita, *Organometallics*, 2013, **32**, 5281–5284; T.-P. Lin and J. C. Peters, *J. Am. Chem. Soc.*, 2013, **135**, 15310–15313; N. Curado, C. Maya, J. Lopez-Serrano and A. Rodriguez, *Chem. Commun.*, 2014, **50**, 15718–15721; M. Yamashita, *Bull. Chem. Soc. Jpn.*, 2016, **89**, 269–281.
- 38 While our manuscript was in review, Osuka and coworkers described several NCN-type subporphyrinatoboron(III) pincer ligands and their complexes with Pd and Pt. These ligands have a BN₃ sub-unit similar to our ^{Ph}TBDPhos and ^{iPr}TBDPhos complexes described here. See: M. Kitano, T. Tanaka and A. Osuka, *Organometallics*, 2017, DOI: 10.1021/acs.organomet.7b00130, ahead of print.
- 39 K. Niedenzu, P. Fritz and J. W. Dawson, *Inorg. Chem.*, 1964, **3**, 1077–1079.
- 40 P. Fritz, K. Niedenzu and J. W. Dawson, *Inorg. Chem.*, 1965, **4**, 886–889.
- 41 E. F. Rothgery and K. Niedenzu, *Synth. Inorg. Met.-Org. Chem.*, 1971, **1**, 117–121.
- 42 G. Schmid, R. Boese and D. Blaeser, *Z. Naturforsch., B: Anorg. Chem., Org. Chem.*, 1982, **37**, 1230–1233.
- 43 G. R. Van Hecke and W. D. Horrocks Jr., *Inorg. Chem.*, 1966, **5**, 1968–1974.
- 44 G. Garton, D. E. Henn, H. M. Powell and L. M. J. Venanzi, *Chem. Soc.*, 1963, 3625–3629.
- 45 D. W. Allen, I. T. Millar, F. G. Mann, R. M. Canadine and J. Walker, *J. Chem. Soc. A*, 1969, 1097–1100.
- 46 J. A. S. Bomfim, F. P. de Souza, C. A. L. Filgueiras, A. G. de Sousa and M. T. P. Gambardella, *Polyhedron*, 2003, **22**, 1567–1573.
- 47 I. B. Sivaev and V. I. Bregadze, *Coord. Chem. Rev.*, 2014, **270–271**, 75–88.
- 48 G. R. Eaton and W. N. Lipscomb, *N.M.R. Studies of Boron Hydrides and Related Compounds*, Benjamin, New York, 1969.
- 49 S. Aldridge, A. J. Downs, C. Y. Tang, S. Parsons, M. C. Clarke, R. D. L. Johnstone, H. E. Robertson, D. W. H. Rankin and D. A. Wann, *J. Am. Chem. Soc.*, 2009, **131**, 2231–2243.
- 50 P. J. Bailey, D. Lorono-Gonzales, C. McCormack, F. Millican, S. Parsons, R. Pfeifer, P. P. Pinho, F. Rudolphi and A. S. Perucha, *Chem. – Eur. J.*, 2006, **12**, 5293–5300.
- 51 I. Morales-Becerril, M. Flores-Alamo, A. Tlahuext-Aca, A. Arevalo and J. J. Garcia, *Organometallics*, 2014, **33**, 6796–6802.
- 52 C. F. Macrae, I. J. Bruno, J. A. Chisholm, P. R. Edgington, P. McCabe, E. Pidcock, L. Rodriguez-Monge, R. Taylor, J. van de Streek and P. A. Wood, *J. Appl. Crystallogr.*, 2008, **41**, 466–470.
- 53 C. D. Good and D. M. Ritter, *J. Am. Chem. Soc.*, 1962, **84**, 1162–1166.
- 54 M. S. Rodriguez-Morgade, C. G. Claessens, A. Medina, D. Gonzalez-Rodriguez, E. Gutierrez-Puebla, A. Monge, I. Alkorta, J. Elguero and T. Torres, *Chem. – Eur. J.*, 2008, **14**, 1342–1350.
- 55 E. Tsurumaki, J. Sung, D. Kim and A. Osuka, *J. Am. Chem. Soc.*, 2015, **137**, 1056–1059.
- 56 M. V. Fulford, D. Jaidka, A. S. Paton, G. E. Morse, E. R. L. Brisson, A. J. Lough and T. P. J. Bender, *Chem. Eng. Data*, 2012, **57**, 2756–2765.
- 57 L. Coue, L. Cuesta, D. Morales, J. A. Halfen, J. Perez, L. Riera, V. Riera, D. Miguel, N. G. Connelly and S. Boonyuen, *Chem. – Eur. J.*, 2004, **10**, 1906–1912.
- 58 J. S. Hartman and G. J. Schrobiligen, *Can. J. Chem.*, 1972, **50**, 713–719.
- 59 H. Li and M. B. Hall, *J. Am. Chem. Soc.*, 2015, **137**, 12330–12342.
- 60 P. A. Dub and J. C. Gordon, *Dalton Trans.*, 2016, **45**, 6756–6781.
- 61 For a review of MLC reactions see: J. R. Khusnutdinova and D. Milstein, *Angew. Chem., Int. Ed.*, 2015, **54**, 12236–12273.
- 62 K. Lee, H. Wei, A. V. Blake, C. M. Donahue, J. M. Keith and S. R. Daly, *Dalton Trans.*, 2016, **45**, 9774–9785.
- 63 G. M. Sheldrick, *Acta Crystallogr., Sect. A: Fundam. Crystallogr.*, 2008, **64**, 112–122.
- 64 O. V. Dolomanov, L. J. Bourhis, R. J. Gildea, J. A. K. Howard and H. J. Puschmann, *Appl. Crystallogr.*, 2009, **42**, 339–341.